Published in final edited form as:
Invest Radiol. 2012 July ; 47(7): 398–405. doi:10.1097/RLI.0b013e31824bd237.

Insonation of Targeted Microbubbles Produces Regions of Reduced Blood Flow within Tumor Vasculature

Xiaowen Hu, Ph.D.[1], **Azadeh Kheirolomoom, Ph.D.**[1], **Lisa M. Mahakian, M.S.**[1], **Julie R. Beegle, B.S.**[1], **Dustin E. Kruse, Ph.D.**[1], **Kit S. Lam, MD, Ph.D.**[2,3], and **Katherine W. Ferrara, Ph.D.**[1]

[1]Department of Biomedical Engineering, University of California, Davis, One Shields Ave, Davis, CA 95616

[2]Department of Biochemistry and Molecular Medicine, UCD Cancer Center, University of California, Davis, Sacramento, CA 95817

[3]Division of Hematology and Oncology, Internal Medicine, UCD Cancer Center, University of California, Davis, Sacramento, CA 95817

Abstract

Objectives—In ultrasound molecular imaging, a sequence of high pressure ultrasound pulses is frequently applied to destroy bound targeted microbubbles in order to quantify accumulated microbubbles or to prepare for successive microbubble injections; however, the potential for biological effects from such a strategy has not been fully investigated. Here, we investigate the effect of high pressure insonation of bound microbubbles and the potential for thrombogenic effects.

Materials and methods—A total of 114 mice carrying either Met-1 or NDL tumors was insonified (Siemens Sequoia system, 15L8 transducer, 5 MHz color-Doppler pulses, 4 MPa or 2 MPa peak-negative pressure, 8.1 ms pulse repetition period, 6-cycle pulse length, and 900 ms insonation). Microbubbles conjugated with cyclic RGD or LXY-3 peptides, or control (no peptide) microbubbles were injected and contrast pulse sequencing (CPS) was used to visualize the flowing and bound microbubbles. An anti-CD41 antibody was injected in a subset of animals to block potential thrombogenic effects.

Results—Following the accumulation of targeted microbubbles and high pressure (4 MPa) insonation, reduced blood flow, as demonstrated by a reduction in echoes from flowing microbubbles, was observed in 20 Met-1 mice (71%) and 4 NDL mice (40%). The area of low image intensity increased from 22 ± 13% to 63 ± 17% of the observed plane in the Met-1 model ($p<0.01$) and from 16 ± 3% to 45 ± 24% in the NDL model ($p<0.05$). Repeated microbubble destruction at 4 MPa increased the area of low image intensity to 76.7 ± 13.4% ($p<0.05$). The fragmentation of bound microbubbles with a lower peak-negative pressure (2 MPa) reduced the occurrence of the blood flow alteration to 28% (5 of 18 Met-1 tumor mice). The persistence of the observed blood flow change was approximately 30 minutes after the microbubble destruction event. Dilated vessels and enhanced extravasation of 150,000 MW FITC-dextran were observed by histology and confocal microscopy. Pre-injection of an anti-CD41 antibody blocked the

Corresponding Author Information: Katherine W. Ferrara Department of Biomedical Engineering University of California, Davis 451 E Health Sciences Dr. Davis, CA 95616 Phone: (530) 754-9436 Fax: (530) 754-5739 kwferrara@ucdavis.edu.

reduction of tumor blood flow, where a reduction in blood flow was observed in only 1 of 26 animals.

Conclusion—High pressure fragmentation of microbubbles bound to tumor endothelial receptors reduced blood flow within two syngeneic mouse tumor models for ~30 minutes. Platelet activation, likely resulting from the injury of small numbers of endothelial cells, was the apparent mechanism for the flow reduction.

Keywords

Bound targeted microbubbles; molecular imaging; microbubble fragmentation; tumor vasculature; platelet aggregation

INTRODUCTION

Thermal and mechanical biological effects induced by ultrasound include changes in vascular and cell membrane properties[1]. Mechanical effects can be produced by inertial cavitation of endogenous gas cores or exogenous microbubbles, or by stretching and compressing tissues. Fluid jets, penetrating through the microbubble and imposing mechanical force onto the adjacent cell surfaces can produce cell membrane damage, apoptosis, hemolysis, and cell-cell junction disruption[2–4]. The frequency and amplitude of transmitted pulses significantly alter the effects of microbubble oscillation[5,6].

In general, greater biological effects are produced by sonication with a lower frequency and a higher peak-negative pressure (PNP). After insonifying circulating microbubbles with a transmitted frequency above 5 MHz, reports of biological effects are mixed: no significant biological effects are observed with 7.5 MHz pulses at a high mechanical index (MI, defined as PNP normalized by the square root of center frequency)[7], while blood-brain barrier (BBB) disruption was observed with a 5.7 MHz center frequency and a 0.3 MI[8]. Pulse repetition frequency (PRF), pulse duty cycle, and treatment time have a significant influence on the generation of biological effects as well. Using a high duty cycle and long pulse duration with circulating microbubbles, imaging pulses from diagnostic systems can trigger vessel disruption and vascular leakage[8–11]. In addition, biological effects increase with increasing microbubble injected dose or concentration. In addition to the acoustic parameters, the generation of biological effects is dependent on tissue properties[12,13]. Tumor blood flow has been shown to be partially or completely blocked after microbubble collapse inside tumor vasculature with both therapeutic ultrasound (HIFU and physiotherapy) and laboratory exposure systems[14–17]. Survival of mouse models of cancer is significantly increased after ultrasound treatment, suggesting a therapeutic effect[14,17]; however, the mechanism has not been fully characterized.

Targeted microbubbles have been shown to accumulate efficiently on vascular receptors *in vitro* and *in vivo*[18–20]. In this study, tumor blood flow is shown for the first time to be locally reduced by the destruction of *targeted, bound* microbubbles through insonation with a high frequency (7 MHz), short pulse length and low PRF sequence transmitted by a commercial diagnostic ultrasound system. We set out to determine the frequency and mechanism of this biological effect.

MATERIALS AND METHODS

1. Mouse tumor models

All animal studies were conducted under a protocol approved by the Institutional Animal Care and Use Committee of the University of California, Davis. A solution of Met-1[21] or

NDL[22] tumor cells (1×10^5 cells in 20 μl of PBS) were injected directly into the 4th inguinal mammary fat pads of the recipient female FVB mouse (6–7 weeks, 25–30 g, Charles River, MA). Met-1 and NDL tumors are demonstrated to be highly metastatic and to produce significant angiogenesis. The mean maximum diameter of scanned tumors (2 weeks after the implantation) was approximately 5 mm. A total of 114 tumor mice were imaged throughout the course of this study, including 10 NDL tumors and 104 Met-1 tumors. The number of mice in each study group is summarized in Table 1. Scanned regions were shaved and treated with depilatory (Veet®; Reckitt Benckiser, Parsippany, NJ). Ultrasound gel (Parker Laboratories, Fairfield, NJ) was used to couple the ultrasound transducer and the skin surface. Throughout the imaging procedure, mice were anesthetized with 2% isoflurane (Halocarbon Laboratory, River Edge, NJ) in oxygen (2 L/min) and were positioned on a heated stage to maintain body temperature.

2. Microbubbles

Visistar® integrin cyclic-RGD (cRGD) microbubbles were provided by Targeson (San Diego, CA). LXY-3 peptide-conjugated and control non-targeted non-biotinylated microbubbles were produced in our laboratory. Biotinylated LXY-3 peptide was conjugated onto biotinylated microbubbles via an avidin/biotin coupling reaction[23]. The size distribution of these three formulations was similar with a mean diameter of ~2 μm and a microbubble concentration of 2×10^9 particles/ml. cRGD microbubbles have a high affinity for the $\alpha_v\beta_3$ integrin in Met-1 tumor vasculature, thus specifically bind to tumor endothelial cells[24]. LXY-3 peptide is a novel cyclic peptide that has also been demonstrated to have a high binding specificity to the $\alpha_3\beta_1$ integrin[25]. Our preliminary data confirm that LXY-3 peptide-conjugated microbubbles specifically accumulate at Met-1 tumor sites (data not shown).

For each injection, 1×10^8 (in 50 μl microbubble diluent) of targeted or control non-targeted microbubbles (without targeting ligands on the distal end of PEG group) were administrated into the tail vein. The peak image intensity resulting from targeted and control microbubbles occurred ~30 seconds after the injection and microbubbles were cleared from the blood stream after 7 minutes. Targeted microbubbles adherent to tumor vasculature demonstrated an extended persistence time in the vasculature (approximately 12 minutes) as compared to flowing microbubbles.

3. Imaging protocols

CPS contrast imaging mode (Sequoia® 512, Siemens, Issaquah, WA; 15L8 transducer, center frequency of 7 MHz) was used to visualize both flowing microbubbles (thus estimating the volume of flowing blood) and bound microbubbles. CPS imaging parameters remained constant during the imaging study with a transmitted acoustic power of 0.09 MI (PNP of 230 kPa), a frame rate of 10 Hz, and a CPS gain of −12 dB. In order to destroy the bound microbubbles, 5 MHz color-Doppler pulses with either a 2 or 4 MPa peak-negative pressure (PNP), a 6-cycle pulse length (1.32 μs), and an 8.1 ms pulse repetition period (PRF = 124 Hz) were delivered for 900 ms. The beam width of destruction pulses in the azimuthal and elevation directions was ~25 mm and ~1 mm. For each study, 30 CPS frames were acquired ~30 seconds after microbubble injection to assess tumor blood flow before applying ultrasound treatment and frame-to-frame averaged with motion tracking.

In a preliminary study in the Met-1 tumor model, 3-second, 30 frames of CPS images at a frame rate of 10 Hz (MI=0.09) were applied at 7.5 minutes after the injection of cRGD-conjugated microbubbles (n=6) and no significant change in image intensity was observed (Fig. 1 a).

To evaluate the effect of the destruction of targeted microbubbles with 4 MPa pulses, Met-1 tumors (n=28) and NDL tumors (n=10) were insonified, while additional Met-1 tumors were insonified with 2 MPa pulses (n=18) (Fig. 1 b). For studies of targeted agents, 7 minutes after injection, freely-circulating microbubbles had cleared from the blood stream, leaving bound microbubbles on tumor vasculature. A second set of 30 frames of CPS images was recorded at this time to represent the presence of bound microbubbles. Destructive ultrasound pulses (double arrows) were then applied once at 7.5 minutes after the first injection and a third set of 30 frames of CPS tumor images was acquired after the destruction pulse to validate the elimination of bound microbubbles in the imaging plane (arrows). Twelve minutes after the first injection, a second dose of targeted microbubbles was injected and a fourth set of 30 frames of CPS images was acquired to assess altered tumor blood flow. A fifth set of 30 frames of CPS images was recorded 19 minutes after the first injection (7 minutes after the second injection) to evaluate the effect of altered tumor blood flow on the binding of targeted microbubbles.

In order to determine whether platelet binding was a portion of the biological mechanism for the decreased flow, in a separate group (n=26), 0.1 mg of an anti-CD41 antibody (BD Bioscience, Franklin Lakes, NJ) was injected intraperitoneally in the Met-1 model 50 minutes before the injection of microbubbles, followed by a 50 μL saline flush (Fig. 1 c). The imaging protocol described above was then applied. With this protocol, 90% of the circulating platelets are deactivated after the injection[26].

To further investigate the effect on the vasculature, 150 μl of FITC-dextran particles with a molecular weight of 150,000 Da and a concentration of 25 mg/ml (Sigma-Aldrich, St. Louis, MO) were injected in a separate group (n=5) at 6.5 minutes after microbubble injection (thus 1 minute before microbubble fragmentation). A second microbubble injection occurred at 8.5 minutes after the initial injection to verify the generation of region of reduced contrast intensity and CPS images were acquired at 0.5 and 9 minutes after the initial injection. Immediately after the second imaging study, the mouse was euthanized and the ultrasound-treated tumor and the bilateral control tumor were excised from the mouse (Fig. 1 d). Tumors were frozen within an Tissue-Tek® O.C.T. compound (Sakura Finetek, Torrance, CA), cryosectioned to 50-μm thickness slices (Leica CM1850 microtome, Germany), mounted with tissue mounting solution (Emsdiasum, Hatfield, PA), and then scanned by confocal microscopy (Axiovert 100; Zeiss, Germany) with a 60× objective lens. The confocal microscope has a laser wavelength of 488 nm and a long-pass 515 nm emission filter. In the same field of view, the fluorescent image was superimposed onto the bright-field image to show both vessels and surrounding cells.

In order to verify the specificity of the observed biological effects with the fragmentation of bound microbubbles, control (non-targeted) microbubbles were administrated into mice implanted with Met-1 tumors (n=10), which were insonified using 4 MPa destructive pulses 2 minutes after injection (Fig. 1 e). CPS images of flowing microbubbles were acquired at 0.5, 1.5, and 2.5 minutes after the initial injection, and 0.5 minute after the second injection (7 minutes after the initial injection).

To study whether the biological effect was enhanced by multiple applications of microbubble destruction, the injection-destruction-injection procedure was repeated in a separate group (n=6) (Fig. 1f). Here, the targeted microbubbles were injected at time 0, 12 and 24 minutes. Destructive ultrasound pulses were applied twice at 7.5 and 19.5 minutes after the first injection and CPS images of flowing microbubbles within the tumor (arrows) were acquired at 7 time points, from immediately after the first injection to immediately after a final injection. The second microbubble injection was used to assess blood flow and to provide targeted microbubbles for the second destructive event.

To study the persistence of the observed change in blood flow, in an additional study (n=5), blood flow was assessed for 40 minutes after bubble injection (Fig. 1 g). Targeted microbubbles were injected at time 0, 12 and 40 minutes. Destructive ultrasound pulses were applied once at 7.5 minutes after the first injection and CPS images of flowing microbubbles within the tumor were acquired at 0.5, 12.5 and 40.5 minutes after the first injection. CPS images of bound microbubbles were acquired at 7 minutes after the first injection. The choice of the 40-minute time period was based on preliminary data.

Image data were recorded digitally and were processed off-line in MATLAB (The MathWorks, Inc., Natick, MA). An amplitude threshold of 15% of the system maximum (of 255) was applied and regions with image intensity below this threshold were considered to be of low image intensity. Wilcoxon rank sum tests were performed to compare the area of reduced contrast intensity in various study groups, with a p value less than 0.05 being considered as significant. Statistical data are presented as mean ± one standard deviation (SD). Based on a sample size calculation, a minimum of 5 animals were required per group to achieve an alpha of 0.05 at a power of 0.8.

4. Histology

H&E staining was performed to observe tumor vascular alterations after ultrasound treatment. Both treated (n=10, the tumors where reduced blood flow was produced after ultrasound treatment) and control tumors (n=10, bilateral untreated tumors) were excised immediately after the second bubble injection (Fig. 1 b) and fixed in formalin solution overnight. On each slide, 6 regions were manually chosen; vessel diameters larger than 1 μm in these regions were measured. The H&E staining plane was chosen as the center of the tumor on ultrasound. In addition, the orientation of the tumor sample was labeled with dye to further assist the co-localization.

RESULTS

Flowing microbubbles within the tumor and surrounding tissue were detected and visualized by CPS contrast imaging 30 seconds after injection, and frame-to-frame averaged over 3 seconds (Fig. 2 a, f, k, and p). Flowing microbubbles had cleared from the blood stream after 7 minutes (Fig. 2 b, g, l, and q); however, targeted microbubbles had accumulated on the tumor vasculature and not on the vasculature of the surrounding normal tissues. The accumulation of RGD-conjugated (targeted to $\alpha_v\beta_3$) and LXY3-conjugated (targeted to $\alpha_3\beta_1$) microbubbles was similar in the Met-1 mouse. The high MI either 4 MPa (Fig. 2 c, h, and r) or 2 MPa (Fig. 2 m) destruction pulses eliminated bound microbubbles in the imaging plane (Fig. 2 b, g, l, and q). Thirty seconds after a second injection of targeted microbubbles, regions devoid of circulating microbubbles were observed on the averaged CPS images (Fig. 2 d and i) and these regions were of a similar area and co-localized with RGD-conjugated (Fig. 2 b) and LXY3-conjugated microbubbles (Fig. 2 g). The application of 4 MPa pulses locally reduced the image intensity in 20 of 28 Met-1 tumors (71%), where the region of low image intensity increased from 22 ± 13% to 63 ± 17% of the tumor region of interest (p<0.01, Fig. 4 a, b. Furthermore, 7 minutes after the second injection, the intensity of bound microbubble echoes was suppressed in the same region observed after the initial injection (Fig. 2 e and j).

Decreasing the destructive pulse pressure from 4 to 2 MPa (Fig. 2 k–o), while keeping other acoustic parameters constant, reduced the occurrence of regions of low contrast intensity from 71% to 28% of 18 Met-1 tumors (Fig. 4 a). In this group, the area with image intensity below the amplitude threshold increased from 25 ± 13% to 57 ± 22% (p<0.01, Fig. 4 b). Both cRGD- (n=8) and LXY-3 (n=10)-conjugated microbubbles were studied and vascular changes were similar for the two ligands.

After the injection of anti-CD41 antibody, LXY-3-conjugated microbubbles accumulated as in other studies but the occurrence of contrast intensity reduction after insonation was only 1 of 26 Met-1 mice (˜4%). Thus, the effect was greatly decreased by the pretreatment (Fig. 2 p–t and Fig. 4 a, b).

In 4 of 10 NDL tumors, regions with reduced image intensity were also observed following the injection of LXY-3-conjugated microbubbles (Fig. 3 a–e). In NDL tumors, the area of the reduced image intensity increased from 16 ± 3% to 45 ± 24% (p<0.05, Fig. 4 b).

Over all studies, the area of the region with reduced image intensity was independent of the intensity of the bound microbubble echoes in the tumor region (Fig. 4 c). On subsequent injections, the contrast image intensity in surrounding tissues was not significantly changed (<10%) after the high MI insonation.

Without the application of high-MI destruction pulses (ie. using CPS only with a PNP below 300 kPa at 7 MHz), locally-reduced tumor blood flow was not observed (data not shown). Similarly, in a study of n=10 Met-1 tumors, the application of destructive pulses to flowing microbubbles (rather than bound microbubbles) did not reduce blood flow with the same acoustic pressure (Fig. 3 f–l and Fig. 4 a, b).

In a separate study, LXY-3-conjugated microbubble injection and destructive insonation were each applied twice to determine whether flow could be further reduced (Fig. 5 a–c). The area of low contrast intensity increased from 45.2 ± 18.4% to 76.7 ± 13.4% (Fig. 5 g) (p<0.05).

Forty minutes after the first injection of microbubbles, LXY-3-conjugated microbubbles were again injected to assay whether flow had returned to baseline. At this time, the extent of the region with low image intensity was 23.5 ± 16.1%, which was approximately the same as the initial measurement before destructive ultrasound pulses (26.8 ± 12.4%) and less than the measurement at 12 minutes (59.8 ± 21.0%). The results suggest that the vasculature recovers from the induced biological effect (Fig. 5 dg).

No obvious histological changes were observed in the tumor interstitium and similarly, hemorrhage was infrequently observed and was not increased by insonation. Vessels with a diameter greater than 1 μm on H&E were quantified. The mean vessel diameter observed on H&E-stained tumors was greater for insonified (17 ± 8 μm) (Fig. 6 a, c) as compared with control tumors (7 ± 4 μm) (Fig. 6 b, c) with the injection of targeted microbubbles. Change in vessel diameter was not found after the destruction of control microbubbles.

In order to further investigate the mechanism for the reduced contrast intensity, fluorescent dextran was injected, allowed to circulate for ˜2.5 minutes, and *ex vivo* slices from the region of interest were evaluated. Confocal images of FITC dextran (green) were superimposed onto the bright-field images (red). Regions of enhanced extravasation were observed in the ultrasound treated tumors (Fig. 6 d). The fluorescent vasculature was visualized in control tumors without significant extravasation within the short period of circulation (Fig. 6 e).

DISCUSSION

In this study, both RGD-conjugated (targeted to $\alpha_v\beta_3$) and LXY3-conjugated (targeted to $\alpha_3\beta_1$) microbubbles accumulated in syngeneic models of breast cancer with a high image contrast ratio. The destruction of bound microbubbles using a high MI, but short duty-cycle pulse sequence created regions with reduced blood flow (as demonstrated by reduced echo intensity) in Met-1 and NDL tumor models. Regions with reduced blood flow were observed

immediately after the destruction of bound microbubbles and resolved within ~30 minutes. The area with reduced blood flow was further enhanced by multiple exposures and can be significantly reduced by decreasing the peak negative pressure of the destruction pulse. Dilated vessels in ultrasound-treated tumors have been reported in studies of non-targeted microbubbles[27]. Here, the leakage of the FITC-dextran particles from the vasculature indicated that gaps between endothelial cells were enhanced after the microbubble destruction.

The hypothesis that the aggregation of the platelets may play an important role in limiting blood flow was verified in this study. The rapid onset of reduced flow after insonation limits the possible mechanisms, eliminating the possibility macrophage recruitment or changes in protein expression. Similarly, the absence of obvious structural changes or hemorrhage upon histology points to a biological amplification of the relatively limited contact between microbubbles and endothelial cells. We and others have previously shown by electron microscopy that endothelial cells can be destroyed by oscillating microbubbles, exposing the basement membrane and increasing vascular permeability[4]. Mechanical damage to the endothelium, particularly with exposure of the basement membrane, has previously been shown to rapidly result in local platelet accumulation[28–30].

With the same acoustic parameters as those applied here to insonify *bound* microbubbles, the destruction of *flowing* microbubbles did not affect blood flow. Thus, with this relatively high ultrasound frequency and low ultrasound pressure, the attachment of microbubbles to the endothelial cell surface was required to affect blood flow. A previous *in vitro* study indicated that microbubble-cell attachment significantly increased the biological effect of a high-power ultrasound exposure[3]. Here, the disorganized and abnormal tumor vessels resulting from tumor angiogenesis[31] were likely to be more sensitive to insonation.

The frequency of occurrence of reduced blood flow was greater in Met-1 than NDL tumors. The vasculature of each of these syngeneic models is similar to human tumors, with enhanced integrin expression and disorganized, leaky vasculature. Met-1 tumors have a higher vascular volume fraction but also demonstrate weak cell-cell adhesion. Thus, we had hypothesized that the effect of ultrasound would be greater and this hypothesis was confirmed here.

The frequency dependence of the effect of ultrasound on tumor vasculature was not investigated in this study due to limitations of the transducer and system. In general, lower frequencies are more likely to produce mechanical effects on surrounding tissues. However, higher ultrasound frequencies improve control of the beam width and treatment region. The duty cycle and the sonication time here were significantly lower than those used in other studies, and were unlikely to generate a thermal effect. The threshold for acoustic parameters required to induce this biological effect should be further investigated. Factors such as the bubble size distribution and the microbubble injection dose could also impact the biological effect, and will be evaluated in future studies in order to decrease or enhance the biological effect. In addition, further study is required to clarify the mechanism underlying the observed reduction in blood flow.

The direct implications of this study suggest that for molecular imaging, bound microbubble destruction should be minimized to avoid potential alterations of the tumor vasculature. Instead of using high PNP destructive pulses to clear bound microbubbles, an extended clearance time or low pressure sonication should be used together with more sophisticated image processing methods[24,32]. Exploitation of reduced tumor blood flow could be used to enhance thermal ablation or to trap therapeutics within the tumor vasculature in a manner similar to trans-arterial chemoembolization.

In conclusion, the rapid destruction of bound microbubbles on the surface of tumor vasculature endothelial cells produced regions with reduced blood flow in two murine tumor models using 5MHz, 1.9MI color-Doppler pulses from a diagnostic system. We hypothesize that oscillating and collapsing microbubbles mechanically disrupt a limited number of endothelial cells, enhancing permeability and exposing the basement membrane.

Acknowledgments

This work is supported by NIH R01CA103828 and R01CA134659.

REFERENCES

1. Feril LB Jr. Kondo T. Biological effects of low intensity ultrasound: the mechanism involved, and its implications on therapy and on biosafety of ultrasound. J Radiat Res (Tokyo). Dec; 2004 45(4): 479–489. [PubMed: 15635256]
2. Brayman AA, Lizotte LM, Miller MW. Erosion of artificial endothelia in vitro by pulsed ultrasound: acoustic pressure, frequency, membrane orientation and microbubble contrast agent dependence. Ultrasound Med Biol. Oct; 1999 25(8):1305–1320. [PubMed: 10576273]
3. Miller DL, Quddus J. Lysis and sonoporation of epidermoid and phagocytic monolayer cells by diagnostic ultrasound activation of contrast agent gas bodies. Ultrasound Med Biol. Aug; 2001 27(8):1107–1113. [PubMed: 11527597]
4. Stieger SM, Caskey CF, Adamson RH, et al. Enhancement of vascular permeability with low-frequency contrast-enhanced ultrasound in the chorioallantoic membrane model. Radiology. Apr; 2007 243(1):112–121. [PubMed: 17392250]
5. Miller DL. Overview of experimental studies of biological effects of medical ultrasound caused by gas body activation and inertial cavitation. Prog Biophys Mol Biol. Jan-Apr;2007 93(1–3):314–330. [PubMed: 16989895]
6. ter Haar G. Safety and bio-effects of ultrasound contrast agents. Med Biol Eng Comput. Aug; 2009 47(8):893–900. [PubMed: 19597745]
7. Miller DL, Dou C, Wiggins RC. Frequency dependence of kidney injury induced by contrast-aided diagnostic ultrasound in rats. Ultrasound Med Biol. Oct; 2008 34(10):1678–1687. [PubMed: 18485567]
8. Bing KF, Howles GP, Qi Y, Palmeri ML, Nightingale KR. Blood-brain barrier (BBB) disruption using a diagnostic ultrasound scanner and Definity in Mice. Ultrasound Med Biol. Aug; 2009 35(8): 1298–1308. [PubMed: 19545939]
9. Miller DL, Pislaru SV, Greenleaf JE. Sonoporation: mechanical DNA delivery by ultrasonic cavitation. Somatic cell and molecular genetics. Nov; 2002 27(1–6):115–134. [PubMed: 12774945]
10. Miller DL, Quddus J. Diagnostic ultrasound activation of contrast agent gas bodies induces capillary rupture in mice. Proc Natl Acad Sci U S A. Aug 29; 2000 97(18):10179–10184. [PubMed: 10954753]
11. Skyba DM, Price RJ, Linka AZ, Skalak TC, Kaul S. Direct in vivo visualization of intravascular destruction of microbubbles by ultrasound and its local effects on tissue. Circulation. Jul 28; 1998 98(4):290–293. [PubMed: 9711932]
12. Jimenez C, de Gracia R, Aguilera A, et al. In situ kidney insonation with microbubble contrast agents does not cause renal tissue damage in a porcine model. J Ultrasound Med. Nov; 2008 27(11):1607–1615. [PubMed: 18946100]
13. Barnett SB, Rott HD, ter Haar GR, Ziskin MC, Maeda K. The sensitivity of biological tissue to ultrasound. Ultrasound Med Biol. 1997; 23(6):805–812. [PubMed: 9300983]
14. Chin C, Raju BI, Shevchenko T, Klibanov A. Control and reversal of tumor growth by ultrasound activated microbubbles. IEEE Ultrasonics Symposium 2009. 2009:77–80.
15. Goertz D, Karshafian R, Hynynen K. Investigating the Effects of Pulsed Low Intensity Ultrasound and Microbubbles in Mouse Tumors. ieee ultrasonics Symposium 2009. 2009:89–92.

16. Wood AK, Bunte RM, Schultz SM, Sehgal CM. Acute increases in murine tumor echogenicity after antivascular ultrasound therapy: a pilot preclinical study. J Ultrasound Med. Jun; 2009 28(6): 795–800. [PubMed: 19470820]
17. Wood AK, Schultz SM, Lee WM, Bunte RM, Sehgal CM. Antivascular ultrasound therapy extends survival of mice with implanted melanomas. Ultrasound Med Biol. May; 2010 36(5):853–857. [PubMed: 20381952]
18. Guenther F, von zur Muhlen C, Ferrante EA, Grundmann S, Bode C, Klibanov AL. An ultrasound contrast agent targeted to P-selectin detects activated platelets at supra-arterial shear flow conditions. Invest Radiol. Oct; 2010 45(10):586–591. [PubMed: 20808239]
19. Anderson CR, Rychak JJ, Backer M, Backer J, Ley K, Klibanov AL. scVEGF microbubble ultrasound contrast agents: a novel probe for ultrasound molecular imaging of tumor angiogenesis. Invest Radiol. Oct; 2010 45(10):579–585. [PubMed: 20733505]
20. Pochon S, Tardy I, Bussat P, et al. BR55: a lipopeptide-based VEGFR2-targeted ultrasound contrast agent for molecular imaging of angiogenesis. Invest Radiol. Feb; 2010 45(2):89–95. [PubMed: 20027118]
21. Borowsky AD, Namba R, Young LJ, et al. Syngeneic mouse mammary carcinoma cell lines: two closely related cell lines with divergent metastatic behavior. Clin Exp Metastasis. 2005; 22(1):47–59. [PubMed: 16132578]
22. Siegel PM, Ryan ED, Cardiff RD, Muller WJ. Elevated expression of activated forms of Neu/ErbB-2 and ErbB-3 are involved in the induction of mammary tumors in transgenic mice: implications for human breast cancer. EMBO J. Apr 15; 1999 18(8):2149–2164. [PubMed: 10205169]
23. Kheirolomoom A, Dayton PA, Lum AF, et al. Acoustically-active microbubbles conjugated to liposomes: characterization of a proposed drug delivery vehicle. J Control Release. Apr 23; 2007 118(3):275–284. [PubMed: 17300849]
24. Anderson CR, Hu X, Zhang H, et al. Ultrasound molecular imaging of tumor angiogenesis with an integrin targeted microbubble contrast agent. Invest Radiol. Apr; 2011 46(4):215–224. [PubMed: 21343825]
25. Yao N, Xiao W, Wang X, et al. Discovery of targeting ligands for breast cancer cells using the one-bead one-compound combinatorial method. J Med Chem. Jan 8; 2009 52(1):126–133. [PubMed: 19055415]
26. Kim MH, Curry FR, Simon SI. Dynamics of neutrophil extravasation and vascular permeability are uncoupled during aseptic cutaneous wounding. Am J Physiol Cell Physiol. Apr; 2009 296(4):C848–856. [PubMed: 19176758]
27. Wood AK, Bunte RM, Cohen JD, Tsai JH, Lee WM, Sehgal CM. The antivascular action of physiotherapy ultrasound on a murine tumor: role of a microbubble contrast agent. Ultrasound Med Biol. Dec; 2007 33(12):1901–1910. [PubMed: 17720299]
28. Ross R, Glomset J, Harker L. Response to injury and atherogenesis. Am J Pathol. Mar; 1977 86(3): 675–684. [PubMed: 842616]
29. Steele PM, Chesebro JH, Stanson AW, et al. Balloon angioplasty. Natural history of the pathophysiological response to injury in a pig model. Circ Res. Jul; 1985 57(1):105–112. [PubMed: 3159504]
30. Davis C, Fischer J, Ley K, Sarembock IJ. The role of inflammation in vascular injury and repair. Journal of thrombosis and haemostasis : JTH. Aug; 2003 1(8):1699–1709. [PubMed: 12911580]
31. Carmeliet P, Jain RK. Angiogenesis in cancer and other diseases. Nature. Sep 14; 2000 407(6801): 249–257. [PubMed: 11001068]
32. Hu X, Zheng H, Kruse DE, Sutcliffe P, Stephens DN, Ferrara KW. A sensitive TLRH targeted imaging technique for ultrasonic molecular imaging. IEEE Trans Ultrason Ferroelectr Freq Control. 2010; 57(2):305–316. [PubMed: 20178897]

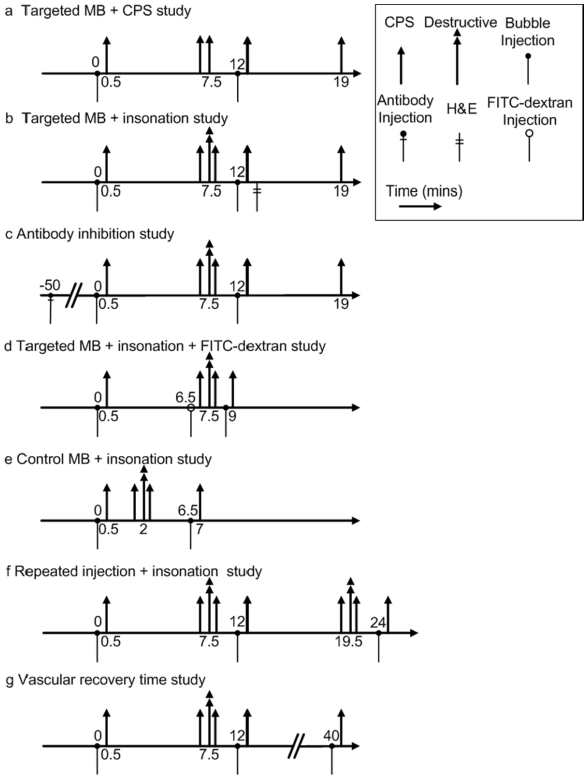

Figure 1.

Pulse sequences employed for studies of targeted microbubbles. (a) Targeted microbubbles + CPS insonation. A 3-second burst of 300 kPa CPS imaging pulses (corresponding to 30 frames of CPS images) insonified bound microbubbles 7.5 minutes after microbubble injection, when the circulating microbubbles were cleared from the blood stream, in order to provide a control study for high amplitude pulses. (b) Targeted microbubbles + high pressure insonation. Destructive pulses were applied to destroy bound microbubbles 7.5 minutes after microbubble injection. (c) The inhibition study aimed to study the mechanism of the biological effect with the addition of an antibody before microbubble injection. (d) Targeted microbubbles + insonation + FITC-dextran. To investigate the effect on the vasculature, FITC-dextran particles were injected 6.5 minutes after the first microbubble injection, which was also 1 minute before microbubble destruction. (e) In a control study, destructive pulses were delivered 2 minutes after microbubble injection. (f) In order to evaluate whether repeated injections produce an additional effect, three injections and two bubble destructions were utilized. (g) In order to evaluate whether the vasculature recovers after this effect, an additional bubble injection and image acquisition were used to estimate the persistence of the biological effect. In each case, 30 frames of CPS images were acquired 30 seconds after microbubble injection, where the intensity of microbubbles in the image plane reached its peak value. Microbubbles were injected before or after the destructive pulses in order to sensitively assess the alteration of tumor blood flow.

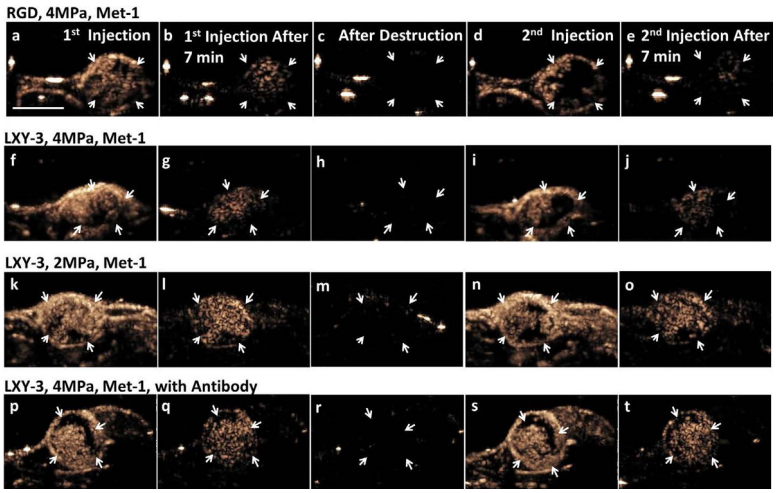

Figure 2.

Four example image sets are shown to represent alteration of Met-1 tumor blood flow in various scenarios. cRGD-conjugated microbubbles were injected in the first row, whereas LXY-3-conjugated microbubbles were injected in the rest rows. Frame-to-frame averaged CPS images were acquired 30 seconds (a, f, k, p) and 7 minutes after the first injection (b, g, l, q), after microbubble destruction at 7.5 minutes (c, h, m, r), and 30 seconds (d, I, n, s) and 7 minutes after the second injection (e, j, o, t), respectively. Orange pixels represent CPS enhancement (the presence of the microbubbles in the imaging plane). With 4 MPa insonation of bound microbubbles, the difference between the averaged CPS images of flowing microbubbles acquired 30 seconds after the first injection (a, f) and the second injection (d, i) delineates the region with a change in blood flow in the tumor region (indicated by white arrows). The generation of additional regions with reduced flow was further verified by comparing the 7-minute CPS images of bound microbubbles between the first (b, g) and the second (e, j) injection. The reduction of tumor blood flow was also observed after bound microbubble destruction by 2 MPa insonation (k–o). With pre-treatment of anti-CD41 antibody 50 minutes before microbubble injection, bound microbubble destruction by 4 MPa insonation did not reduce tumor blood flow (p–t). The scale bar represents 5 mm.

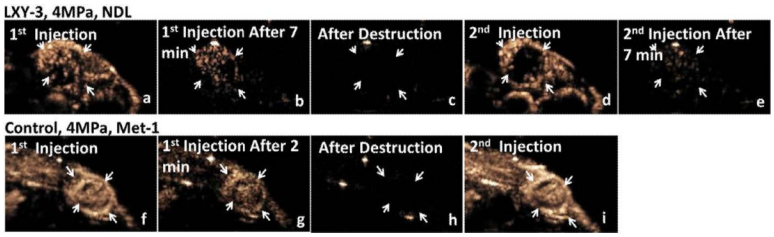

Figure 3.

Two example image sets are shown to demonstrate the dependence of the observed biological effect on tumor tissue and the attachment of targeted microbubbles onto endothelium cells. (a–e) An example of regions of reduced blood flow using 4 MPa destruction pulses with LXY-3-conjugated microbubbles in NDL tumors. Compared to the pre-treatment images (a), additional regions with low echo intensity were observed in the tumor (d) after the bound microbubbles were destroyed (b, c). The echo intensity of bound microbubbles (e) decreased in regions where echoes from flowing agents were reduced (d). White arrows indicate regions of reduced contrast image intensity. (f–i) With the destruction of control non-targeted flowing microbubbles (g, h), no additional region of low blood flow was observed on CPS images of flowing microbubbles acquired before and after flowing microbubble destruction (f, i). The scale bar represents 5 mm.

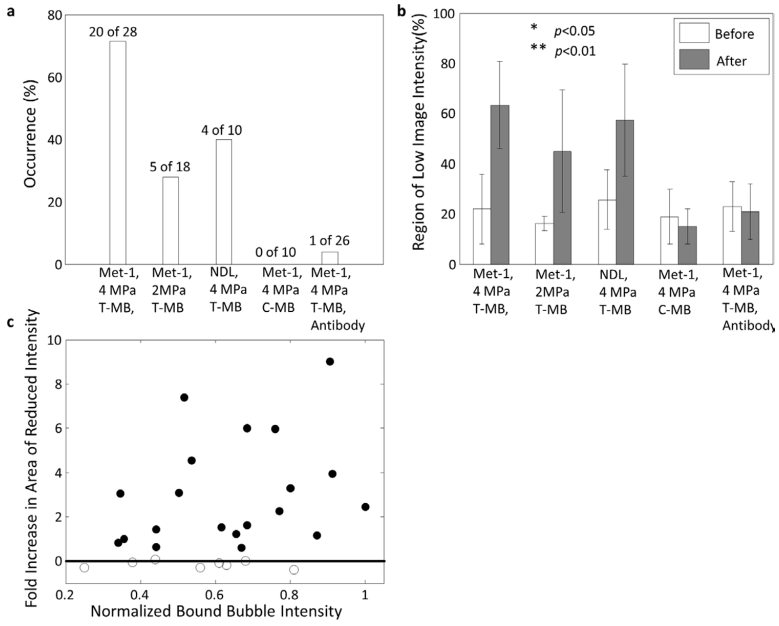

Figure 4.

The occurrence and area of regions with reduced contrast image intensity in Met-1 and NDL tumors with two acoustic pressures with data combined between cRGD and LXY3-conjugated microbubbles. (a) Using 4 MPa-PNP pulses, regions of reduced flow were observed in 71% of 28 Met-1 and 40% of 10 NDL tumors. Using 2 MPa-PNP pulses, regions of reduced flow were observed in 28% of 18 Met-1 tumors. Using 4 MPa-PNP pulses to destroy flowing non-targeted microbubbles, regions of reduced flow were not observed in 10 Met-1 tumors. With pre-treatment by anti-CD41 antibody, reduced blood flow was produced in 1 of 26 insonified Met-1 tumors (4%). (b) The area with reduced contrast intensity before and after bound microbubble destruction. For a 4 MPa pulse pressure, the area of reduced flow increased from 22 ± 13% to 63 ± 17% ($p<0.01$) in Met-1 tumors and 16 ± 3% to 45 ± 24% ($p<0.01$) in NDL tumors by destruction of bound targeted microbubbles. For Met-1 tumors and a 2 MPa pulse pressure the area with reduced flow increased from 25 ± 13% to 57 ± 22% ($p<0.05$). With the destruction of flowing non-targeted microbubbles, the area of reduced contrast intensity was not significantly increased. Similarly, in the inhibition study, the area of regions with reduced contrast intensity was unchanged when platelet adhesion was blocked. (c) The increased area with low contrast image intensity before and after microbubble destruction was independent of the echo intensity generated by bound microbubbles within the local region.

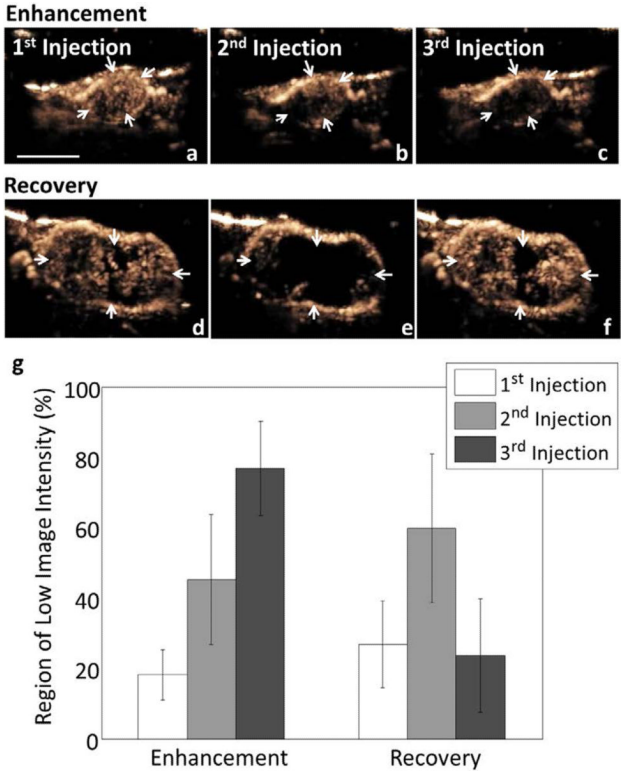

Figure 5.

Summary of the effect of multiple targeted microbubble injections (a–c, g), the time required for vascular recovery (d–f, g). Multiple injections of LXY-3-conjugated microbubbles, each followed by insonation, increased the area with reduced blood flow (a–c). Tumor (arrows) images were acquired before microbubble destruction (a), after the first microbubble destruction (b) and after the second microbubble destruction (c). The area with reduced echo intensity increases significantly after each application of destructive insonation (g). Evaluating vascular recovery after insonation demonstrated that regions with low contrast intensity following microbubble destruction recovered ˜40 minutes after the first microbubble injection (d–f). LXY-3-conjugated microbubbles were injected at time 0, 12 and 40 minutes. Destructive ultrasound pulses were applied once at 7.5 minutes after the first injection and CPS tumor images (arrows) were acquired at 0.5 (d), 12.5 (e) and 40.5 minutes after the first injection (f). The area with reduced echo intensity increased after microbubble destruction but returned to the initial level after ˜30 minutes (g). * indicates $p<0.05$. The scale bar represents 5 mm.

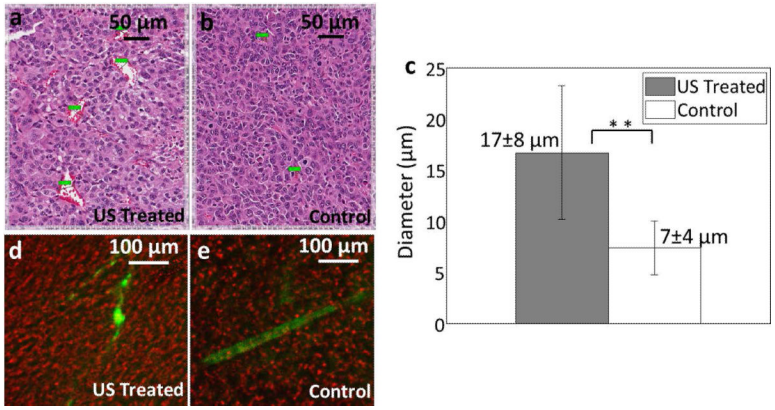

Figure 6.

Histological and confocal results for the insonation of bound microbubbles. (a, b) H&E of insonified (a) and control (b) Met-1 tumors from mice that had been injected with LXY-3-conjugated microbubbles. (c) Summary of vessel diameter assessed from H&E, combining studies with Met-1 and NDL tumors and LXY-3 and RGD-conjugated microbubbles. The mean diameter of vessels was greater in the ultrasound-treated tumors (17 ± 8 μm) as compared with control tumors (7 ± 4 μm). (d, e) Confocal images from control and insonified tumors from mice that had been injected with LXY-3-conjugated microbubbles. FITC-Dextran (green) overlaid on bright field image (red). Insonified tumors (d) include unevenly distributed FITC-dextran which has extravasated. In control tumors (e), discrete blood vessels are visualized. ** indicates $p<0.01$ (e). Scale bar in a and b represents 50 μm; while scale bar in d and e represents 100 μm.

Table 1

Study groups

	Met-1 (LXY-3)	Met-1 (cRGD)	Met-1 (non-targeted)	NDL (LXY-3)	Total
1. Targeted + CPS, 300 kPa	0	6	0	0	6
2. Targeted + insonation, 4 MPa	20	8	0	10	38
3. Targeted + insonation, 2 MPa	10	8	0	0	18
4. Non-targeted + insonation, 4 MPa	0	0	10	0	10
5. Repeated injection (targeted + insonation), 4 MPa	6	0	0	0	6
6. Recovery time, 4 MPa	5	0	0	0	5
7. Histology	3 (out of Group 2)	4 (out of Group 2)	0	3 (out of Group 2)	10
8. Dextran-fluorescence imaging (targeted + insonation)	5	0	0	0	5
9. Anti-CD41 antibody inhibition (targeted + insonation)	26	0	0	0	26